International Journal of Electrical Components and Energy Conversion
2015; 1(5): 92-101
Published online December 30, 2015 (http://www.sciencepublishinggroup.com/j/ijecec)
doi: 10.11648/j.ijecec.20150105.11
ISSN: 2469-8040 (Print); ISSN: 2469-8059 (Online)

Robust Design and Control of Linear Actuator Dedicated to Stamping Press Application

Souhir Tounsi

National School of Electronics and Telecommunications of Sfax, SETIT-Research Unit, Sfax University, Sfax, Tunisia

Emailaddress:
souhir.tounsi@enetcom.rnu.tn

To cite this article:
Souhir Tounsi. Robust Design and Control of Linear Actuator Dedicated to Stamping Press Application. *International Journal of Electrical Components and Energy Conversion.* Vol. 1, No. 5, 2015, pp. 92-101. doi: 10.11648/j.ijecec.20150105.11

Abstract: In this paper, we present a robust design and control approach of all converter-linear actuator dedicated to Stamping Press Application. The linear actuator is designed by a systemic design approach taking in account the constraints of the application such as displacement limit and interactions between the design and the control. The model developed is implanted under the simulation environment Matlab / Simulink. The obtained results encourage the industrialization of the studied structure of the Stamping Press Machine.

Keywords: Stamping Press, Linear Motor, Design, Modeling, Finite Element, Simulations

1. Introduction

Several research works address the problem of design and variable speed driving of linear motors for industrial applications requiring an accuracy of the position and speed of the movable shaft [1-3]. These studies have shown several drawbacks of linear motors stepping and variable reluctance those which may be mentioned [1-3]:

- Vibration.
- Average precision of the position control.
- Complication control algorithms of reluctance linear motors since the inductance is variable depending on the position the movable shaft.

Our application is to automate a Stamping Press to make repetitive cycles to transform pieces of sheet metal in average thickness in parts to be used in industrial applications such manufacturing of the yokes of the electric machines. Our choice was directed on an innovated linear motor cylindrical type structure with permanent magnets. This type of motor is with concentrated winding to reduce congestion and inductance of winding heads. The procedure for manufacturing of this type of actuator is easy to automate. The control law chosen is a scalar type control to monitor the speed and moving force of the movable shaft, it is following robust in front of view simplicity and precision of the speed and position control. The movable shaft carries the sheet metal punch tool.

In this context, this paper presents a systemic design and modeling methodology of the actuator resting on works carried out in [4-7].

2. Sizing of the Linear Actuator

2.1. Analytical Sizing of the Actuator

The linear motor structure with permanent magnets is illustrated by figure 1:

a. Motor cutting plane b. Front view of the motor

Figure 1. *Linear motor structure.*

Several research studies show that the analytical method is recommended for the design of electrotechnical devices, since it leads to sizing models highly parameterized and compatible thereafter for large optimization problems. In addition, certain factors need to be adjusted by the finite element method which can be cited as an example the coefficient of leakage flux. This method is also based on well-justified simplifying assumptions. For this, we set to establish an analytical model adjusted by the finite element method. The method chosen is then an hybrid Analytic / Finite Element method. This method combines the advantages of the analytical method as

compatibility with large optimization programs and advantages of the finite element method such that accuracy of the results [5-15].

2.2. Modeling of the Actuator

The motor is controlled by a DC-AC converter with two voltage levels controlled in current by pulse width modulation. The converter feed voltage is derived from a three-phase rectifier connected to a three-phase 220 V / 380 V-50 Hz sector.

The average rectified voltage is estimated by the following equation:

$$U_{dc} = \frac{3 \times \sqrt{3} \times V_{max}}{\pi} \quad (1)$$

Where V_{max} is maximal phase voltage of the sector.

Le actuator electric constant is expressed by the flowing relation:

$$K_e = 2 \times L_{ra} \times N_{sph} \times B_e \quad (2)$$

Where L_{ra} is the width of the width of the radial opening of the magnets in meter, N_{sp} is the phase number of turns and B_e is the flux density in the air-gap.

The maximal value of the back electromotive force is expressed by the following relation:

$$E = K_e \times V \quad (3)$$

Where V is the velocity of the movable stem.

We deduce the expression of the electromagnetic force of attraction of the moving stem:

$$F_{em} = 2 \times L_{ra} \times N_{sph} \times B_e \times I \quad (4)$$

Where I is the maximal phase current.

The average length of a coil turn is expressed by the following relation:

$$L_{sp} = 2 \times \left(\left(\frac{D_{cm}}{2} + H_a + e + \frac{H_d}{2} \right) \times \alpha \times \pi + L_{enc} \right) + 2 \times \left(\left(\frac{D_{cm}}{2} + H_a + e + \frac{H_d}{2} \right) \times A_{dentm} + L_{enc} \right) \quad (5)$$

Where D_{cm} is the movable stem diameter, e is the air-gap thickness, H_a is the magnet thickness, H_d is the tooth height, α is the tooth opening coefficient in the radial direction, L_{enc} is the slot width and A_{dentm} is the angular teeth opening in the axial direction.

We deduce the expression of the phase resistance in function of the temperature of copper:

$$R = r_{cu}(T_c) \times N_{sph} \times L_{sp} \times \frac{\frac{I_{dim}}{\sqrt{2}}}{\delta} \quad (6)$$

Where r_{cu} is the copper resistivity, I_{dim} is the dimensioning current and δ admissible current density in the copper.

An average value of resistance is considered for a copper temperature maintained constant equal to 80°C, assuming that the motor is cooled by a cooling system controlled in temperature (the temperature of the copper equal to 80°C) by acting on the thermal convection coefficient of the refrigerated fluid.

The phase inductance is expressed by the following relation:

$$L = \mu_0 \times \frac{N_d}{3} \times \frac{N_{sph}^2}{\left(\frac{N_d}{3} \right)^2} \times \left(\frac{\frac{S_d}{2}}{2 \times (H_a + e)} \times C_{td} + \frac{L_m \times H_d}{L_{enc}} + \frac{L_d \times H_d}{L_{enc}} \right) \quad (7)$$

Where N_d is the total number of teeth, S_d is the teeth section, C_{td} is a coefficient taking into account the three dimensional effects, L_m is the width of the radial opening of the tooth and L_d is the tooth width in the axial direction.

The phase mutual inductance is expressed by the following relation:

$$M = \mu_0 \times \frac{N_d}{3} \times \frac{N_{sph}^2}{\left(\frac{N_d}{3} \right)^2} \times \left(\frac{\frac{S_d}{2}}{2 \times (H_a + e)} \times C_{td} \right) \quad (8)$$

The C_{td} coefficient is identified by a two-dimensional finite element model of the motor after a cutting along an horizontal plane passing through the axis of the actuator. The model is obtained by spreading the two portions of the actuator.

3. Finite Element Validation of the Analytical Model

3.1. Finite Element Model of the Actuator

The actuator is studied in two dimensions basing on the following assumptions:

- Three-dimensional effects are neglected since the radial opening of the teeth and the magnets is important.
- The motor is axially symmetrical, only half of the actuator is investigated.
- Mesh refinement in the air gap to increase the accuracy of calculations.
- The problem is solved by varying the static position of the movable axis of a step size equal to 26.66 mm by Maxell-2 D software.

With all these assumptions, the two-dimensional model of actuator with refined mesh is shown in Figure 2.

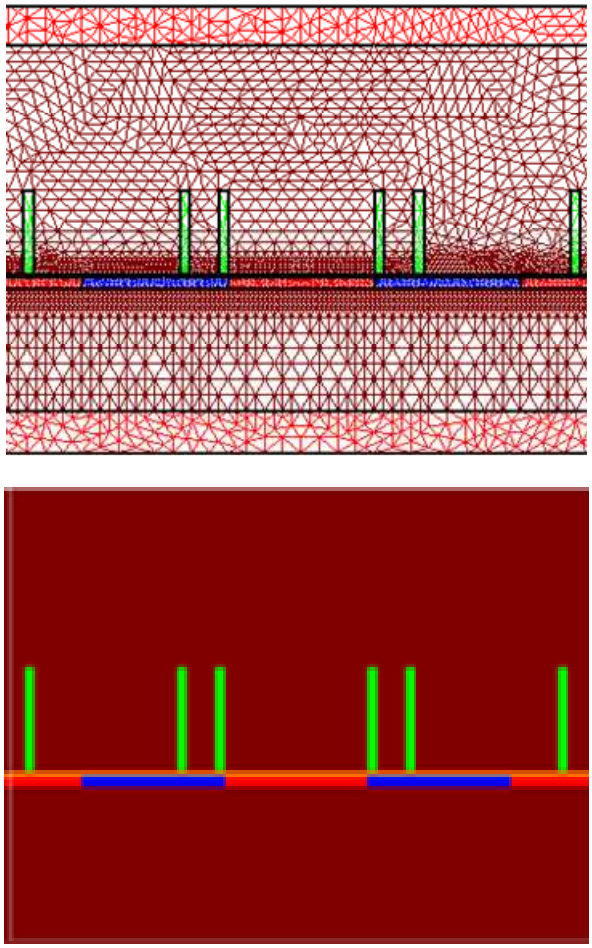

Figure 2. *2 D model of the motor.*

The distribution of field lines at load in the planar portion of the actuator is shown in Figure 3:

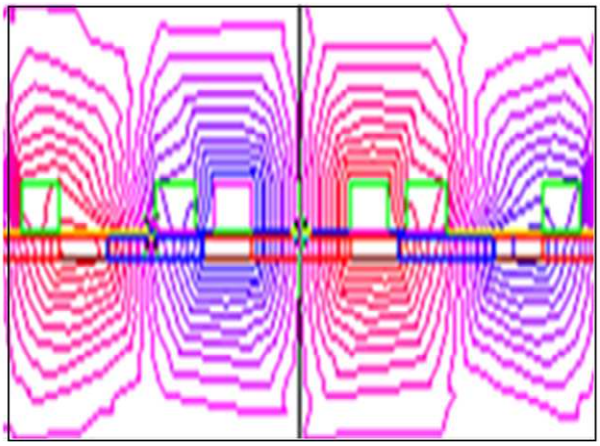

Figure 3. *Field lines at load in the two planar portions of the actuator.*

3.2. Simulation Results

The three phase fluxes a load captured by one coil calculated by finite element method are illustrated by Figure 4:

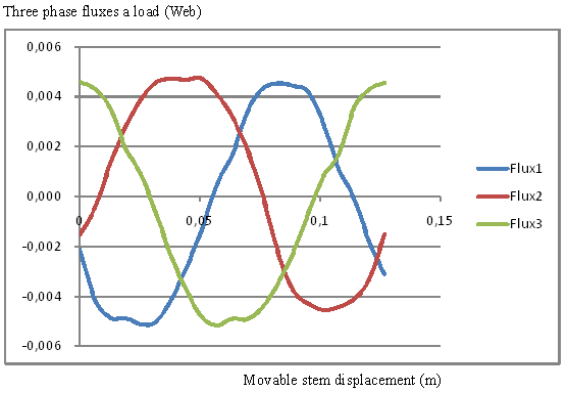

Figure 4. *Three phase fluxes a load captured by one coil in function of the movable stem displacement calculated by finite element method.*

The fluxes are close in form and value of those estimated analytically which validates the analytical design procedure.

The back electromotive forces a load for movable stem speed equal to 2 m/s calculated by finite element method are illustrated by Figure 5:

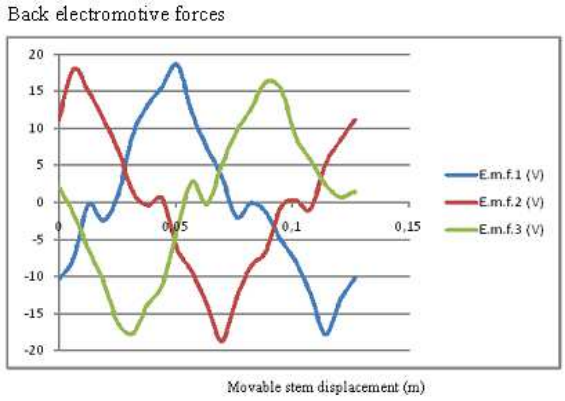

Figure 5. *Back electromotive forces in function of the movable stem displacement calculated by finite element method.*

The back electromotive forces are close in form and value of those estimated analytically which validates the analytical design procedure.

The electromagnetic strength calculated by finite element method related to a current value equal to 200 A is illustrated by Figure 6:

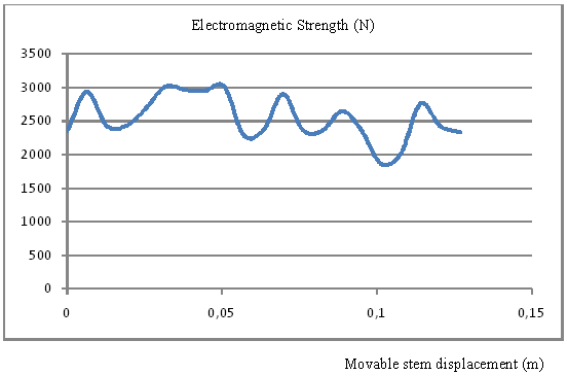

Figure 6. *Electromagnetic strength in function of the movable stem displacement calculated by finite element method.*

The electromagnetic strength is close in form and value of that estimated analytically which validates the analytical design procedure entirely.

4. Motion Equation

The vehicle motion equation is derived from the fundamental relationship of dynamics:

$$M_m \times \frac{dV}{dt} = F_{em} + F_p - F_f - F_{mec} - F_{pr}(d) \quad (9)$$

M_m is the movable stem mass, V is the movable stem velocity, F_{em} is electromagnetic attraction strength, F_p is the gravity strength, F_f is the strength due to iron losses, F_{mec} is the strength due to mechanical losses, F_{pr} is the Stamping Press resistance force and d is the movable stem displacement.

The movable stem displacement is deducted from the following relation:

$$d = \int V \times dt \quad (10)$$

The gravity strength is expressed by the following relation.

$$F_p = M_m \times g \quad (11)$$

Where g is considered equal to 9.8 $N.kg^{-1}$.

The strength due to iron losses is expressed by the following relation [6-26]:

$$F_f = \mathrm{sgn}(F_{em}) \times \frac{1.1 \times \left(\frac{f}{50}\right)^{1.5} \times \left(M_{ds} \times B_d^2 + M_{cs} \times B_{cs}^2\right)}{\frac{V}{R_e}} \quad (12)$$

Where f is the frequency of the stator currents, M_{ds} is the mass of the stator teeth, M_{cs} is the mass of the stator yoke, B_d is the flux density in the teeth and B_{cs} is the flux density in the stator yoke.

The strength due to mechanical losses is expressed by [6-26]:

$$F_{mec} = \mathrm{sgn}(F_{em}) \times \left(s + n_u \times \mathrm{abs}(V) + x_{si} \times V^2\right) \times \frac{1}{R_e} \quad (13)$$

Where s is the dry friction coefficient, nu is the viscous friction coefficient, xsi is the fluid friction coefficient and Re is the movable stem bore radius.

The motion equation is implanted under the simulation environment Matlab / Simulink according to Figure 7.

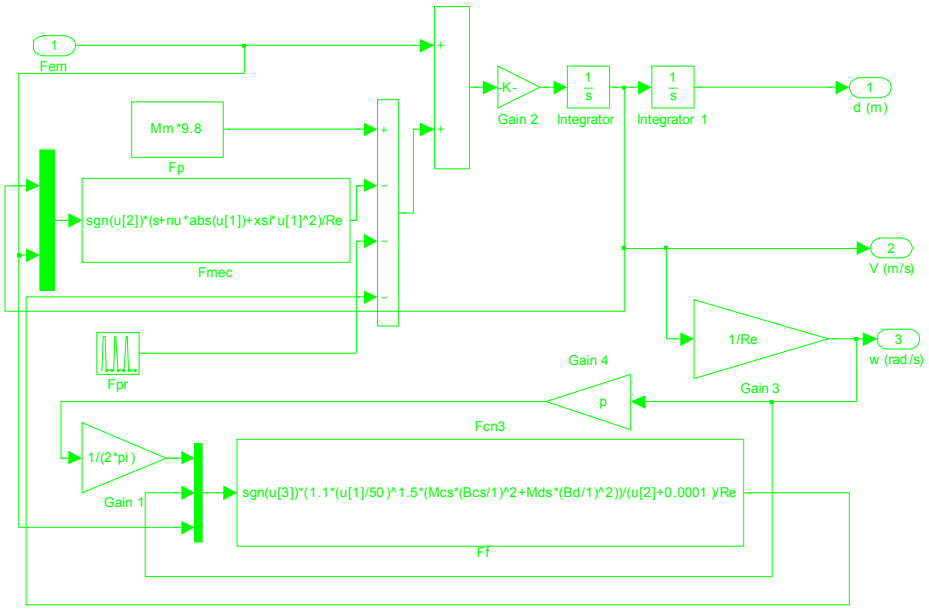

Figure 7. *Simulink model of the motion equation.*

5. Speed Control

The speed comparator outputs the amplitude of the reference currents minimizing the error between the reference speed and the response speed. Indeed, the reference speed is compared to the response speed. The comparator output drives a proportional / integral controller type (PI) to provide the amplitude of reference currents minimizing the speed error. The Simulink model of the speed controller is shown in Figure 8 [6-26].

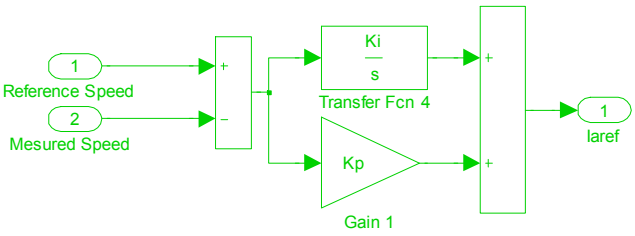

Figure 8. *Simulink Model of the speed regulator.*

6. Current Regulation

Regulators currents allow the imposition of currents having the same shape and in phase with the back electromotive forces. Indeed, the reference currents are compared to the phase currents of the actuator. The outputs of the three comparators attack three proportional / integral (PI) regulators to provide three reference voltages necessary to impose ideal currents in phase with the back electromotive forces and to minimize the error between the reference speed and response speed of the movable stem [6-26].

Simulink model of the current regulator is illustrated in Figure 9:

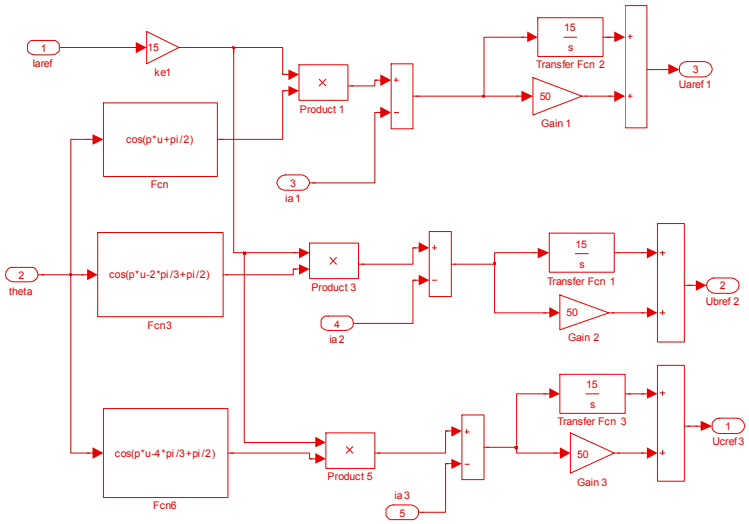

Figure 9. *Simulink model of the currents regulator.*

7. Model of the Back Electromotive Forces

The back electromotive forces are expressed by the three following equations [6-26]:

$$e_1 = K_e \times V \times \cos\left(p \times \frac{V}{R_e} \times t + \frac{\pi}{2}\right) \quad (14)$$

$$e_2 = K_e \times V \times \cos\left(p \times \frac{V}{R_e} \times t - \frac{2\times\pi}{3} + \frac{\pi}{2}\right) \quad (15)$$

$$e_3 = K_e \times V \times \cos\left(p \times \frac{V}{R_e} \times t - \frac{4\times\pi}{3} + \frac{\pi}{2}\right) \quad (16)$$

Where K_e is the electric constant of the motor and V is the linear velocity of the motor and p is the number of pole pairs.

These equations are implanted under Matlab-Simulink environment according to Figure 10:

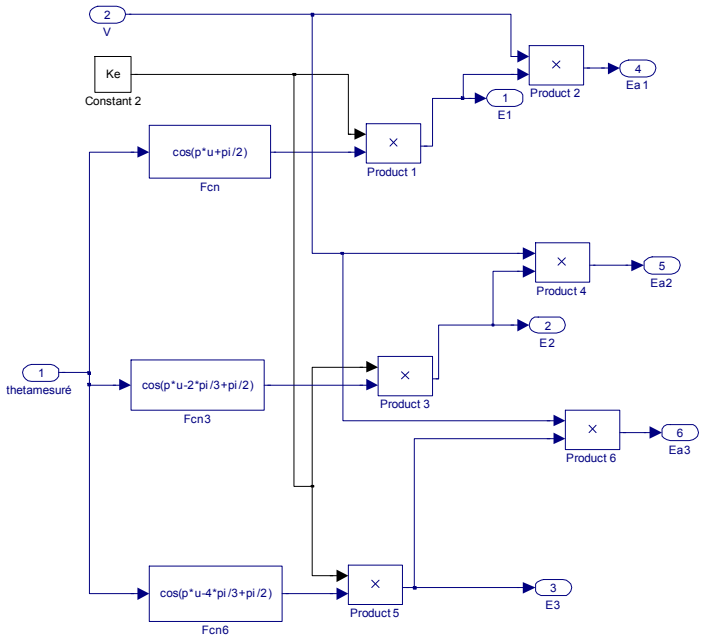

Figure 10. *Simulink model of the back electromotive forces.*

8. Generator of Control Signals

The control signal generator compares the three reference voltages to a triangular signal having a frequency much greater than the voltages provided by the regulators of the currents. The output of each comparator drives an hysteresis variant between 0 and 1 to reproduce the control signals of the IGBT 1, 3 and 5. The speed controller and current controller adjusts the pulse width of the control signals so as to impose currents in phase with the back electromotive forces and to minimize the error between the reference speed and the speed of response. The control signals of the IGBT 2, 4 and 6 are respectively complementary to the control signals of IGBT 1, 3 and 5 to avoid short circuit, the control pulses of S2, S4 and S6 are shortened to avoid duplication between two control signals of an arm. The Simulink model of the control signals generator is illustrated by Figure 11:

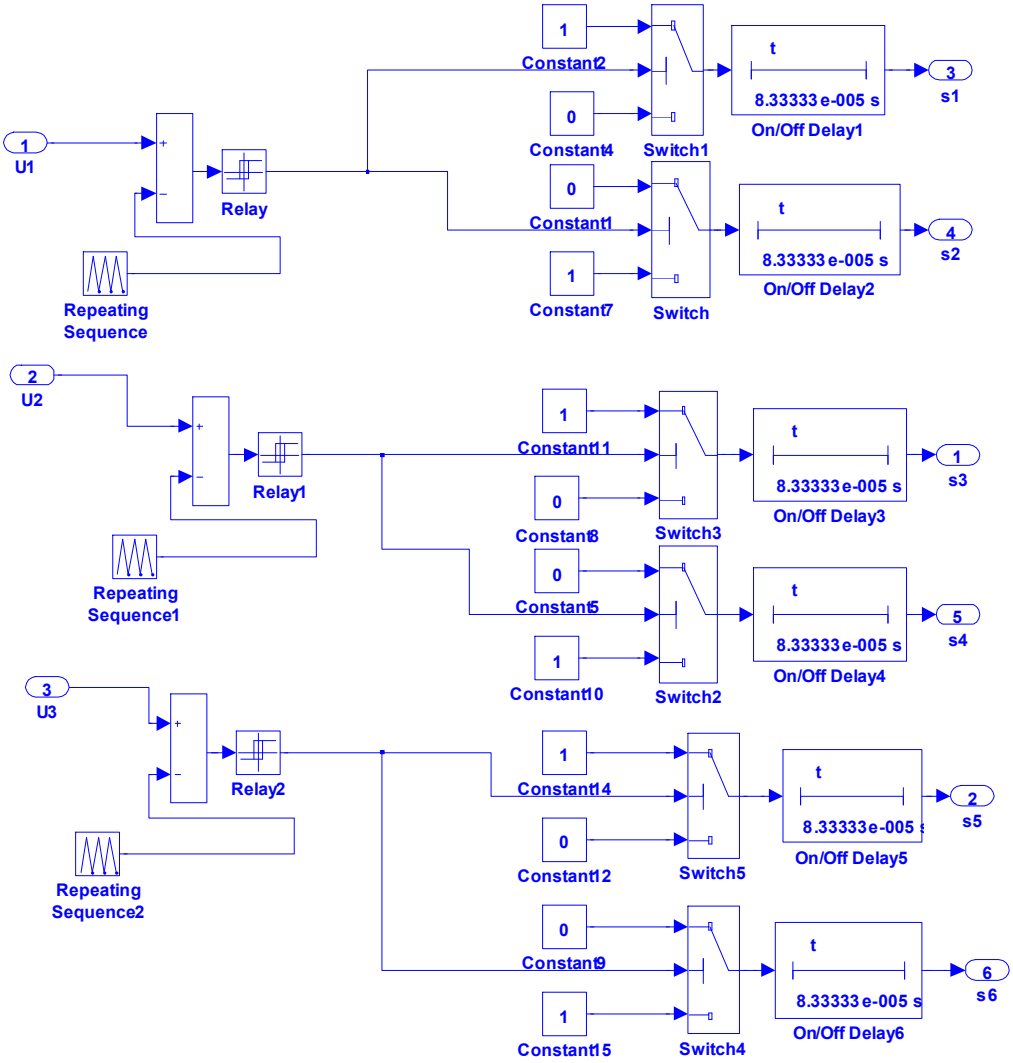

Figure 11. *Simulink Model of the control signals generator.*

9. Model of the Motor-Converter

The motor is powered by a two-level voltage inverter with IGBTs. Each phase of the motor is equivalent to a resistor in series with an inductance and a back electromotive force.

The three phases models of the motor are described by the following equations:

$$V_1 = R \times i_1 + (L - M) \times \frac{di_1}{dt} + K_e \times V \times \cos\left(p \times \frac{V}{R_e} \times t + \frac{\pi}{2}\right) \quad (17)$$

$$V_2 = R \times i_2 + (L - M) \times \frac{di_2}{dt} + K_e \times V \times \cos\left(p \times \frac{V}{R_e} \times t - \frac{2 \times \pi}{3} + \frac{\pi}{2}\right) \quad (18)$$

$$V_3 = R \times i_3 + (L - M) \times \frac{di_3}{dt} + K_e \times V \times \cos\left(p \times \frac{V}{R_e} \times t - \frac{4 \times \pi}{3} + \frac{\pi}{2}\right) \quad (19)$$

Where R, L, M and K_e are respectively the resistance, inductance, mutual inductance and the motor electric constant, ii and Vi are the current and the voltage of the phase i.

The electromagnetic torque is given by the following relation:

$$F_{em} = \frac{1}{V}(e_1 \times i_1 + e_2 \times i_2 + e_3 \times i_3) \quad (20)$$

Where ei is the back electromotive force of the phase i.

The model of the motor-converter is implanted under the Matlab-Simulink according to Figure 12:

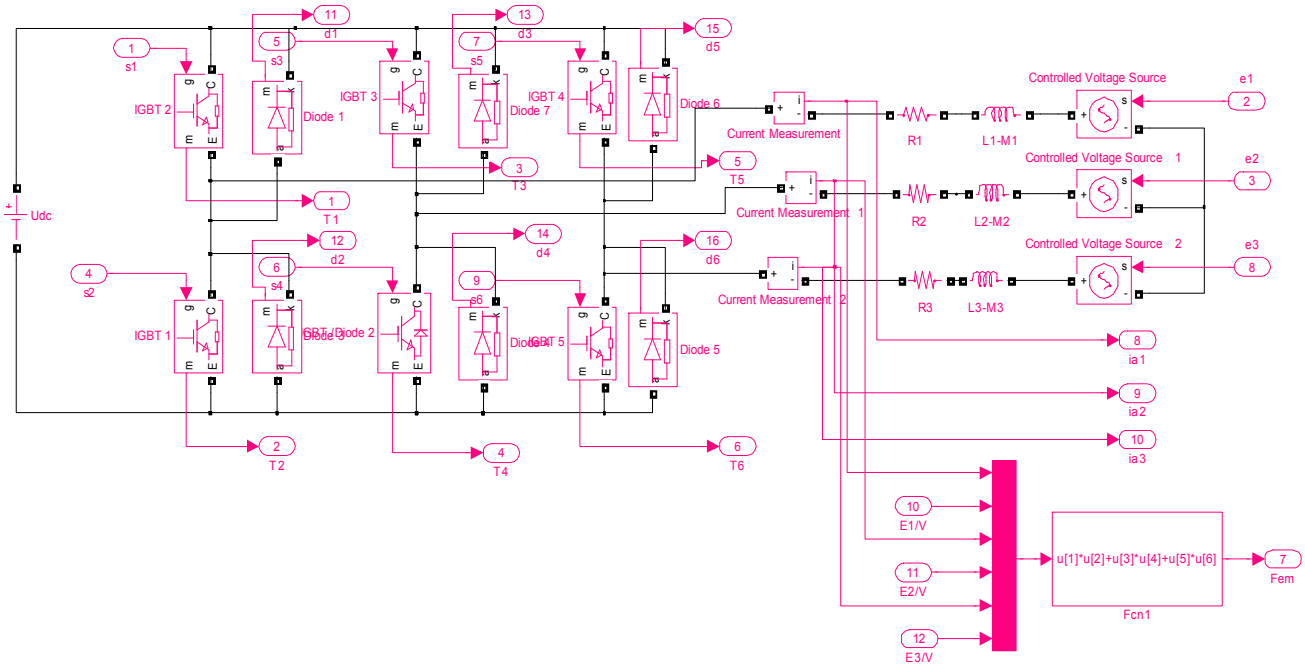

Figure 12. Simulink Model of the motor-converter.

10. Global Model of the Power Chain

The coupling of different models of the power system leads to the global model implanted under the Matlab / Simulink simulation environment according to Figure 13:

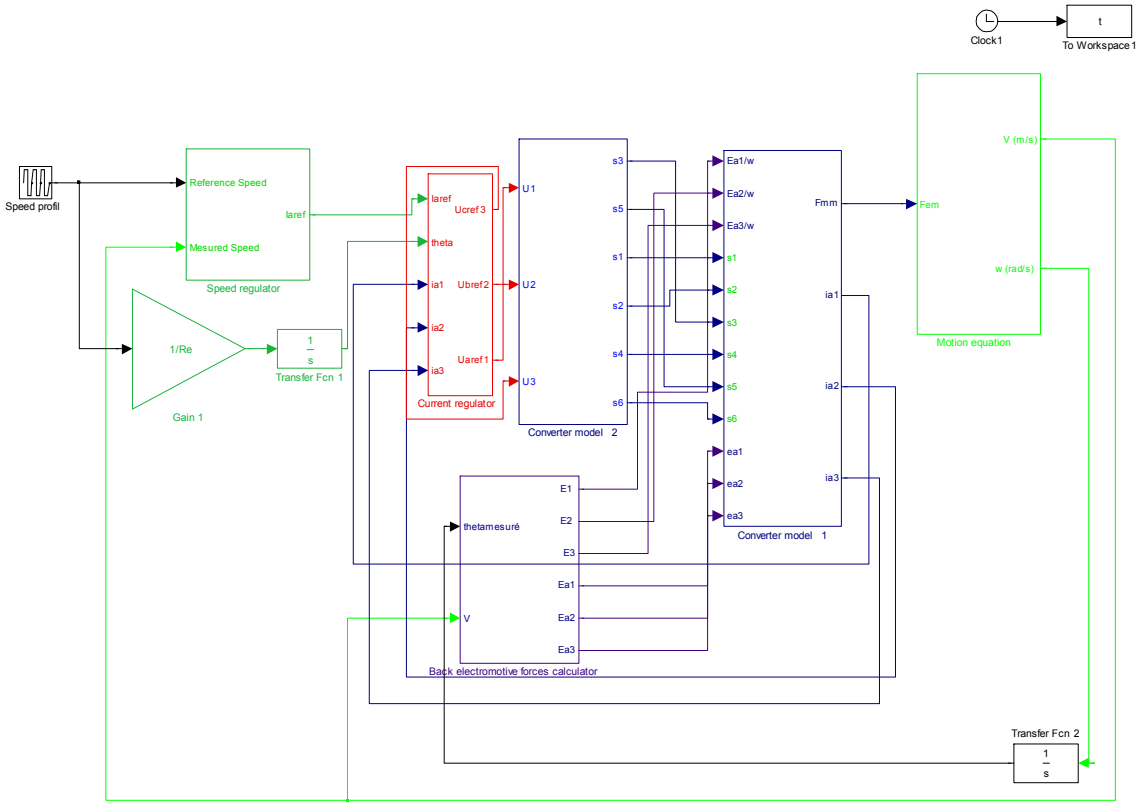

Figure 13. Simulink model of the global system.

11. Description of the Simulation Results

The simulation parameters (Table 1) are extracted from the developed design and modeling program of the studied power system.

Table 1. *Simulation parameters.*

Parameters	Values	Units
Movobale stem mass (Mm)	102.371	kg
Switching frequency (fsw)	20	Hz
Phase inductance (L)	3.663	mH
Phase mutual inductance (M)	0.199	mH
Rotor resistance (R)	3.624	mΩ
Number of pole paires (p)	4	/
Electric constant (Ke)	9.602	Volt/(rad/s)
DC bus voltage	514.6	Volt
Flux density in the air-gap (Be)	0.85	Tesla
Flux density in stator yoke (Bcs) and rotor yoke (Bcr)	1.6	Tesla
Flux density in the teeth (Bd)	1.02	Tesla
Stator yoke mass (Mcs)	108.989	Kg
Teeth mass (Mds)	318.179	Kg

The response speed of a stamping cycle is shown in Figure 14:

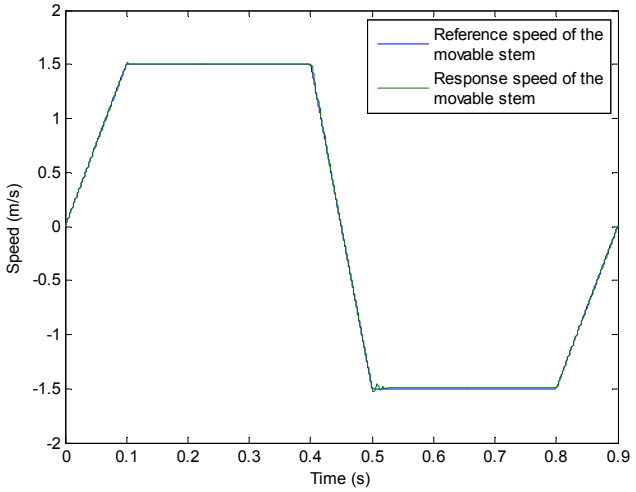

Figure 14. *Response speed of a stamping cycle.*

Figure 14 shows that the response speed follow with good accuracy the stamping cycle, which shows the performance of the selected technique of control.

Figure 15 illustrates the displacement of the movable stem:

Figure 15 shows that the displacement of the movable stem is accurate, since it joined to its return the initial position exactly (d = 0 m).

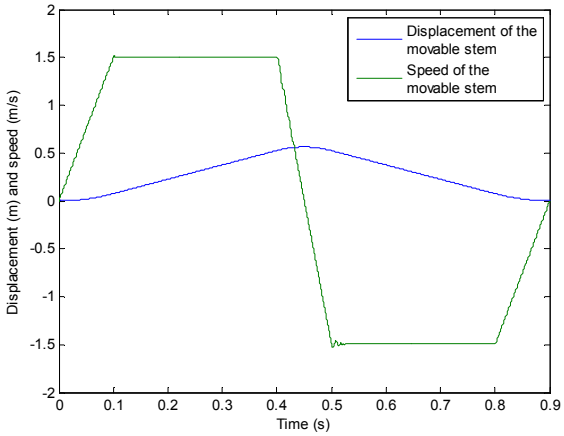

Figure 15. *Displacement of the movable stem.*

Figure 16 illustrates the evolution of the three phase currents:

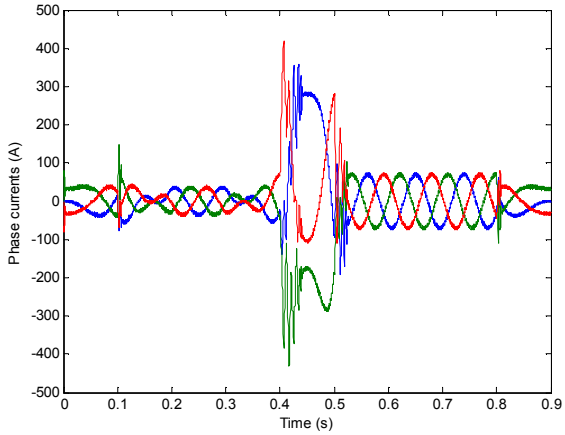

Figure 16. *Three phase currents.*

Figure 16 show that the phase currents present their strong values during the phase of gone up since the gravity strength is important.

Figure 17 shows the change of the back electromotive force compared to the phase current:

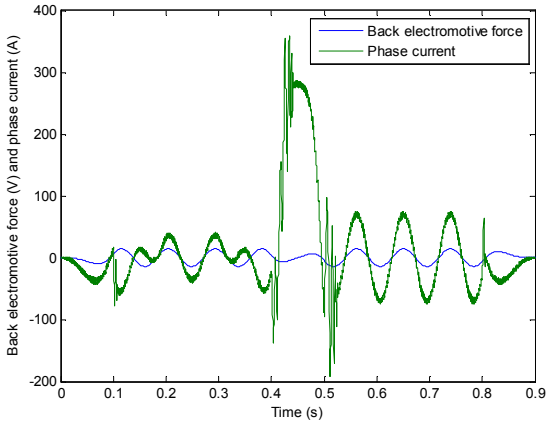

Figure 17. *Change of the back electromotive force compared to the phase*

current.

The phase shift between the current and the electromotive force is very low leading to a significant reduction in the energy consumed. This characteristic shows the effectiveness of the developed control technique.

The figure 18 shows the evolution of the electromagnetic strength and the resistance strength:

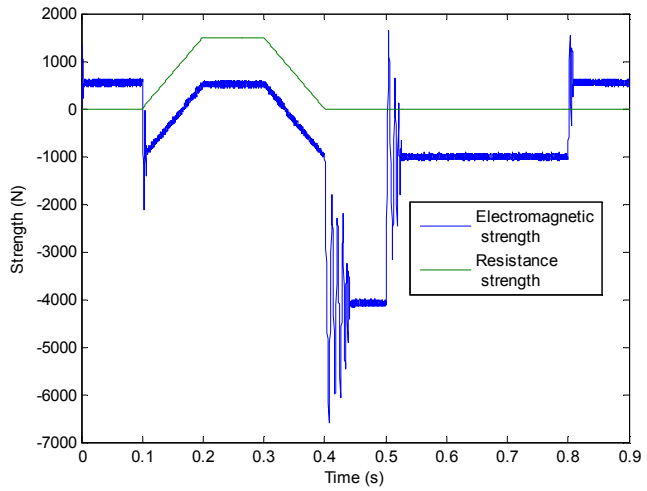

Figure 18. *Evolution of the electromagnetic strength and the resistance strength.*

During the attack phase of the sheet, the electromagnetic strength becomes positive and important to overcome the stamping strength resistance.

Figure 19 illustrates the evolution of the electromagnetic power:

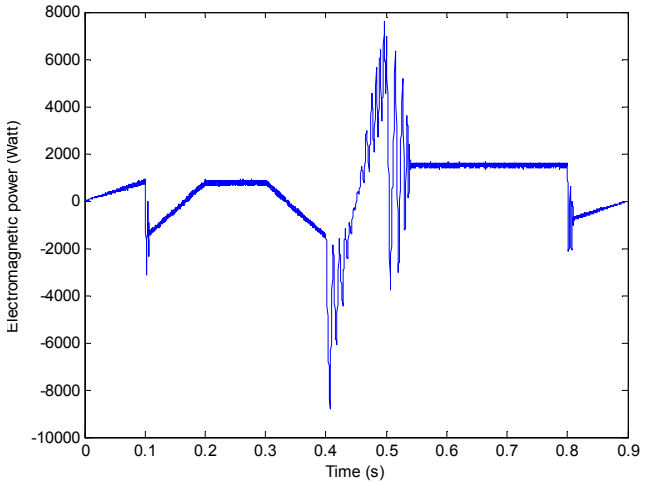

Figure 19. *Evolution of the electromagnetic power.*

Figure 19 show that the electromagnetic power present their strong values during the phase of gone up since the gravity strength is important. During the attack phase of the sheet, the electromagnetic power becomes positive and important to overcome the stamping resistance strength.

Figure 20 illustrates the evolution of the losses strengths:

Figure 20 shows that the strengths due to iron losses and mechanical losses are negligible, which shows the performance of the developed design approach.

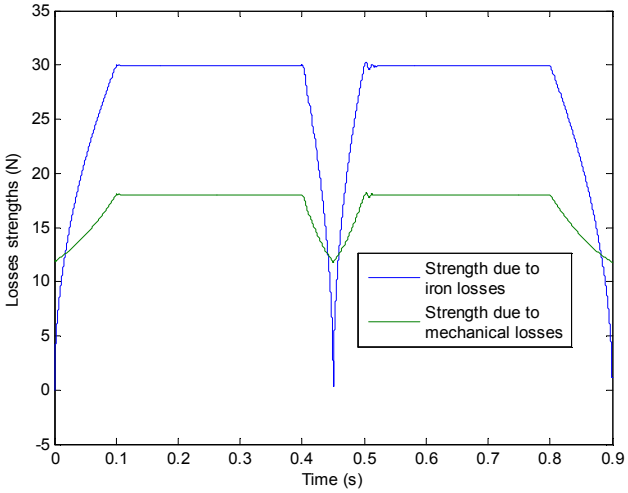

Figure 20. *Evolution of the losses strengths.*

12. Conclusion

In this paper is shown a comprehensive approach of robust design and control of a linear motor with permanent magnets dedicated to Stamping Press Application. A design model of the linear motor based on joint method analytic / finite element is developed. This model takes into account the constraints of the application and the interactions between the control and the sizing of the actuator. The model developed can be applied to several industrial applications other than the present application. This model is also highly parameterized, and eventually leads to problems of optimization of large dimensions. One proposed solution to the automation of Stamping Press is presented.

This study is completed by the development of a robust control law. Simulation results are with good scientific level, leading to the full validation of the design and control approach.

As prospects, it will be very interesting to industrialize this innovative product.

References

[1] Choi, C. and T.-C. Tsao (2005). "Control of linear motor machine tool feed drives for end milling: Robust MIMO approach." Mechatronics 15(10): 1207-1224.

[2] Dahl, P. R. (1976). "Solid friction damping of mechanical vibrations." AIAA Journal 14(12): 1675-82.

[3] Denkena, B., H. K. Tonshoff, X. Li, J. Imiela and C. Lapp, "Analysis and control/monitoring of the direct linear drive in end milling." International Journal of Production Research, 2004, 42(24): 5149-66.

[4] Souhir Tounsi, Systemic Design of Electric Vehicles Power Chain Optimizing the Autonomy, Accepted for publication by Journal of Electrical Engineering (JEE), Indexed in SCOPUS.

[5] Souhir Tounsi, Systemic Design and Optimization Improving Performances of Permanent Magnet Motors, International Journal of Electrical Components and Energy Conversion. Vol. 1, No. 1, 2015, pp. 1-15. Doi: 10.11648/j.ijecec.20150101.11.

[6] Ajmia Belgacem, Mariem Ben Amor, Souhir Tounsi. Trapezoidal Control Based on Analytical and Finite Element Identification of Axial Flux Brushless DC Motor Dedicated to Electric Traction. International Journal of Electrical Components and Energy Conversion. Vol. 1, No. 1, 2015, pp. 16-23. doi: 10.11648/j.ijecec.20150101.12.

[7] Mariem Ben Amor, Ajmia Belgacem, Souhir Tounsi. Optimal Design and Control of Electric Vehicles Power Chain with Electromagnetic Switch. International Journal of Electrical Components and Energy Conversion. Vol. 1, No. 1, 2015, pp. 24-35. doi: 10.11648/j.ijecec.20150101.13.

[8] Amal Suilah, Nadia Graja, Amal Boudaya, Souhir Tounsi, Modelling of Synchronous Generation System for Renewable Energy, International Journal of Electrical Components and Energy Conversion. Vol. 1, No. 1, 2015, pp. 36-43. doi: 10.11648/j.ijecec.20150101.14.

[9] Marwa Sellami, Souhir Tounsi. Control of Axial Flux DC Motor with Permanent Magnet Dedicated to Electric Traction.International Journal of Electrical Components and Energy Conversion. Vol. 1, No. 1, 2015, pp. 44-48. doi: 10.11648/j.ijecec.20150101.15.

[10] Moez Hadj Kacem, Souhir Tounsi, Rafik Neji. Losses Modeling of the Electric Vehicles Power Chain. International Journal of Electrical Components and Energy Conversion. Vol. 1, No. 2, 2015, pp. 49-54. doi: 10.11648/j.ijecec.20150102.11.

[11] Zaineb Gorbel, Yamina Chihaoui, Nader Barg, Mounir Yahyaoui, Souhir Tounsi. Modelling Approach of Electric Cars Autonomy. International Journal of Electrical Components and Energy Conversion. Vol. 1, No. 2, 2015, pp. 55-62. doi: 10.11648/j.ijecec.20150102.12.

[12] Souhir Tounsi. Electro-thermal Modeling of Permanent Magnet Synchronous Motor. International Journal of Electrical Components and Energy Conversion. Vol. 1, No. 2, 2015, pp. 63-68. doi: 10.11648/j.ijecec.20150102.13.

[13] Houcine MAROUANI and Souhir TOUNSI: Design of a Coiled Rotor Synchronous Motor Dedicated to Electric Traction. Journal of Electrical Systems (JES), Volume 10, Issue 3, (September 2014), Indexed in SCOPUS.

[14] Souhir TOUNSI, Ibrahim BEN SALAH and Mohamed Salim BOUHLEL: Design and control of axial flux Brushless DC motor dedicated to Electric traction. Journal of Automation & Systems Engineering (JASE), Volume 8, Issue 2, (June 2014).

[15] Ajmia BEGACEM, Mohamed Amine FAKHFAKH and SouhirTOUNSI: «OPTIMAL DESIGN AND CONTROL OF ELECTRIC VEHICLE POWER CHAIN» Journal of Electrical Engineering (JEE), Edition 2, juin 2015, Indexed in SCOPUS.

[16] S. TOUNSI "Losses of the electromagnetic modeling and IGBT converters," International Int. J. Electric and Hybrid Vehicles (IJEHV)-Indersciences publisher, Vol. 5, No. 1, 2013, pp: 54-68.

[17] M. Hadj Kacem, S. and R. TOUNSI NEJI "Optimization of Cutting Frequency Electromagnetic Interuptor" International Journal of Computer Applications (0975 - 8887) Volume 67-No.21, April 2013, pp: 23-27.

[18] S. TOUNSI "Comparative study of trapezoidal and sinusoidal control of electric vehicle power train," International Journal of Scientific & Technology Research (IJSTR), Vol. 1, Issue 10, November 2012.

[19] M. Hadj Kacem, S. TOUNSI, R. NEJI "Systemic Design and Control of Electric Vehicles Power Chain," International Journal of Scientific & Technology Research (IJSTR), Vol. 1, Issue 10, November 2012.

[20] S. TOUNSI "Control of the Electric Vehicles Power Chain with Electromagnetic Switches Reducing the Energy Consumption," Journal of Electromagnetic Analysis and Applications (JEMAA) Vol. 3 No. 12, December 2011.

[21] S. TOUNSI Mr. Hadj Kacem and R. NEJI "Design of Static Converter for Electric Traction" International Review on Modelling and Similations (IREMOS) Volume 3, N. 6, December 2010, pp. 1189-1195, Indexed in SCOPUS.

[22] S. TOUNSI and R. NEJI: "Design of an Axial Flux Brushless DC Motor with Concentrated Winding for Electric Vehicles", Journal of Electrical Engineering (JEE), Volume 10, 2010 - Edition: 2, pp. 134-146. Indexed in SCOPUS.

[23] S. TOUNSI, R. NEJI, and F. SELLAMI "Design Methodology of Permanent Magnet Motors Improving Performance of Electric Vehicles", International Journal of Modelling and Simulation (IJMS), Volume 29, No. 1, 2009.

[24] Mr. CHAIEB, S. TOUNSI, R. and F. NEJI SELLAMI: "Design and optimization of axial permanent magnet machines for electric vehicle", Journal of Electrical Systems (JES) Volume 5, issue1, 2009, pp. 17-31, Indexed in SCOPUS.

[25] B. Ben Salah, A. MOALLA, S. TOUNSI, R. and F. NEJI SELLAMI "Analytic Design of a Permanent Magnet Synchronous Motor Dedicated to EV Traction With A Wide Range of Speed Operation", International Review of Electrical Engineering (IREE), Volume 3, No. 1 January - February 2008, Indexed in SCOPUS.

[26] R. NEJI, S. TOUNSI and F. SELLAMI: "Contribution to the definition of a permanent magnet motor with Reduced Production cost for the electrical vehicle propulsion," European Transactions on Electrical Power (ETEP), 2006, 16 pp. 437-460, Indexed in Thomson reuters.